Spectroscopy of very high Q whispering gallery modes in silica microspheres.

The Q of the whispering gallery modes of silica microspheres was measured at 670 nm and 1319 nm. Q's of up to 4.4±0.2x10^9 at 670 nm and 1.5 ± 0.2 x10^8 at 1319 nm were observed. As previously documented, at 670 nm the microsphere Q dropped to ~10^9 over the course of ~ 2 minutes, indicating the adsorption of a monolayer of water onto the surface of the silica. The drop observed in water limited Q from 670 nm to 1319 does not agree with the increase in attenuation expected from bulk water, suggesting a chemically adsorbed monolayer theory. A model of the water saturated Q, linearly dependent on diameter, was developed. A linear relationship between sphere diameter and water saturated Q was observed. This thesis is the final chapter in three years of work regarding the factors limiting microsphere Q. Previous results were published in "High-Q measurements of fused silica microspheres in the near infrared" by David W. Vernooy, Vladimir S. Ilchenko, Hideo Mabuchi, Erik Streed, and H. Jeff Kimble in Vol. 23, No. 4 issue of ***Optics Letters*** *published February 15, 1998*

Erik Streed
Senior Thesis Experimental

May 6, 1999

Advisor
Caltech Professor of Physics H. Jeff Kimble

Contents

Introduction 1

Chapter 1 Optical Attenutaion in fused silica

1.1 Optical attenuation in materials 2
1.2 Scattering in the glassy state 2
1.3 Optical and physical properties of silica 3
1.4 The silica surface 3
1.5 Effects of water on the surface of silica. 4

Chapter 2 Whispering Gallery Modes of dielectric spheres

2.1 Analytic solutions for fields in a dielectric sphere 5
2.2 Series solutions for resonant frequencies 8
2.3 Efficient coupling to Whispering Gallery Modes 9
2.4 Resonator quality of Whispering Gallery Modes 11

Chapter 3 Experimental

3.1 Experimental factors limiting maximum microsphere Q 12
3.2 Microsphere fabrication techniques 14
3.3 Apparatus and measurement methods 16
3.4 Measurements and observations 18
3.5 Discussion 21

Conclusion 23

Acknowledgment 24

References 25

Attachments

Color Plate

"High-Q measurements of fused silica microspheres in the near infrared" by David W. Vernooy, Vladimir S. Ilchenko, Hideo Mabuchi, Erik Streed, and H. Jeff Kimble in Vol. 23, No. 4, issue of **Optics Letters** published February 15, 1998.

Introduction

The whispering gallery modes (WGM) of silica microspheres present a novel optical cavity which offer several advantages over the alternatives. Whispering gallery modes were first observed in the acoustic regime, where two people in a domed room could hear each other clearly across the hall at certain locations. In the 1940's, the whispering gallery modes of dielectric microwave resonators were first investigated. Production of high purity, very low loss (< 0.2 dB/km at 1550 nm) silica offered the opportunity to create an optical solid state resonator of high quality and sub centimeter size. The small mode volume, variable coupling, and high Q make them an attractive device for investigating cavity quantum electrodynamics and nonlinear phenomena. The narrow linewidth, long photon storage, and compact size of silica microspheres make them appealing for use in laser diode stabilization schemes, optical delay lines, narrow line optical filters, and microlasers.

In the near infrared "communications band" between 1310 and 1570 nm, material limited resonantor quality is predicted to be ~10^{11}. Material limited Q's of $8x10^9$ have already been observed in millimeter scale spheres at 633 nm. Measurements at longer wavelengths, and with smaller spheres have failed to reach this material limit. Evidence points towards two surface effects as limiting the Q: a monolayer of chemically adsorped water and sub wavelength surface roughness. These processes are not well understood. Previously published work during my 1997 SURF measured the surface roughness of a microsphere, leading to a paper in Optics Letters as mentioned in the Abstract. The consequences of those results are summarized in the experimental section. Strong evidence in the visible and very near infrared point towards a monolayer of water on the silica surface spoiling the Q of a microsphere minutes after fabrication. Further understanding of this water layer is the goal of this thesis.

Chapter 1

Optical attenuation in fused silica

1.1 Optical attenuation in materials

Consider a beam of light propagating through a volume of real dielectric material. The intensity is gradually diminished by absorption and scattering. Absorption occurs as the light slightly excites UV electronic and far infrared vibrational resonances within the material. In addition, impurities in the material can have resonances with a disproportionately strong impact on the absorption. A pure sapphire crystal (Al_2O_3) is naturally clear, but the introduction of Cr^{+3} ions introduces a strong ruby red resonance. Scattering results from small, subwavelength scale variations in density. Other novel scattering processes occur when light scatters off of a molecular or lattice vibrational mode. These are normally weak phenomena that are difficult to observe.

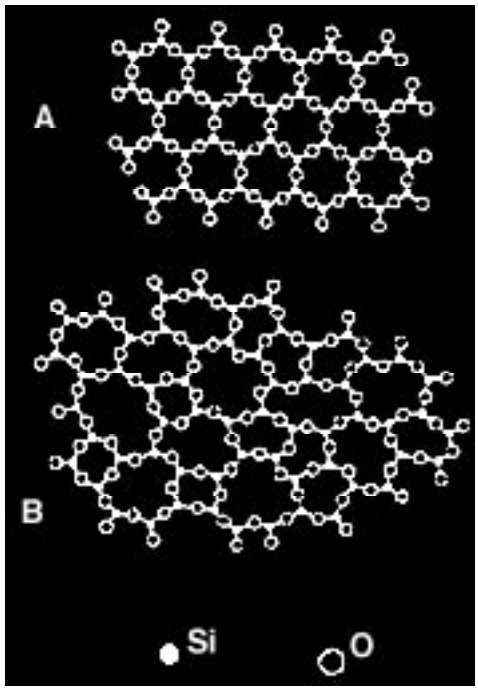

Fig 1.1 Crystalline (A) and amorphous silica (B). Ref. 4.

1.2 Scattering in the glassy state

Glass is an incredibly viscous liquid which, under normal conditions, appears to be a solid. Unlike most other materials, glass does not exhibit a sharp temperature dependent phase transition as it is cooled from the liquid state. Unlike a supercooled fluid, glass does not crash out into a crystalline or polycrystalline form. Glass behaves this way because as it is cooled from a liquid state, the energy associated with making and breaking the silicon oxygen bonds far exceeds the energy gained from the atoms ordering themselves in a regular fashion. This leads to glasses' amorphous structure [Fig 1.1]. The glass temperature T_g describes the transition region when the viscosity increases dramatically. It is important because thermally driven density fluctuations are "frozen" in at this temperature. However this transition is a dynamic property, dependent on how slowly and uniformly the glass is cooled. The slower and more uniform the cooling, the lower T_g and hence the scattering is.

$$\alpha_{scat} = \frac{8\pi^3}{3}\frac{1}{\lambda^4}\left(n^8 p^2\right)\left(k_B T\right)\beta_T$$

Eq 1.1 Attenuation due to scattering. Ref 1. Eq. 1

This is the formula for attenuation by scattering in bulk media, also known as Rayleigh scattering, where k_B is Boltzman's constant, n the materials' index of refraction, λ is the wavelength in question. The glass temperature T_g (~1450K) is used instead of the environmental temperature. β_T is the isothermal compressibility of the material (~ $8x10^{12}$ cm^2/dyne), how the volume changes under pressure at a constant temperature. The photoelastic coefficient $p= (n^2-1)(n^2+2)/(3n^4)$ converts density into dielectric constant fluctuations.

Table 1.1, Useful properties of silica.

$\Delta n/\Delta T = 1.28x10^{-5}$ per °C (0 to 700 °C)
Thermal expansion coefficient = $5.5x10^{-7}$ per °C
Specific Heat (25°C) = 0.177 cal/gm °C
Density (at 25°C) = 2.20 gm/cc

1.3 Optical and physical properties of silica.

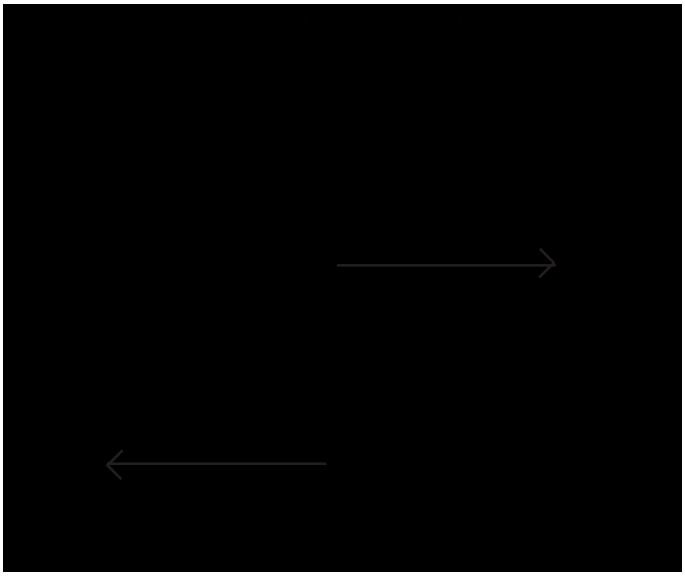

Fig 1.2 Dispersion and absorption curves for silica 300-1700 nm. Compiled from Ref 1, 3, 5.

Table 1.2 Optical constants of water and silica. From Ref 1,2,3, and 5.

λ (nm)	n_{silica}	α_{silica} [m^{-1}]	n_{water}	α_{water} [m^{-1}]
633	1.457	1.61×10^{-3}	1.332	0.363
670	1.456	9.3×10^{-4}	1.331	0.395
852	1.452	4.6×10^{-4}	1.329	4.33
1064	1.450	1.8×10^{-4}	1.326	17.7
1319	1.447	6.5×10^{-5}	1.322	153
1550	1.444	4.6x10-5	1.318	799

$$n(\lambda)^2 - 1 = \frac{0.6961663\lambda^2}{\lambda^2 - (0.0684043)^2} + \frac{0.4079426\lambda^2}{\lambda^2 - (0.1162414)^2} + \frac{0.8974794\lambda^2}{\lambda^2 - (9.896161)^2}$$

Eq. 1.2 Dispersion formula for silica, at 20°C. Accurarte to $\pm 10^{-4}$. Ref 3.

1.4 The silica surface

Bulk silica is not particularly reactive chemically. It is very slightly soluble in water, and somewhat soluble in hydrofluoric acid. The latter reaction creates a solution of SiF_6^{-2} by replacing oxygen near the surface with fluorine . Fluorine can sustain only one bond, and so en masse removes the silicon's connection to the network. The surface chemistry of silica is well understood, because of the use of high surface area silica gels and powders in chemistry. Silica exchange columns are a mature technology which exploit the swapping of surface bound hydroxides with a cation of interest, the hydroxide being analytically measurable. In low concentrations, treatments with HF gas have rendered silica gels hydrophobic by converting surface silinol groups to Si-F [Ref. 1.6].

A freshly prepared anhydrous silica surface quickly acquires a silinol character, with the conversion of bonded oxygen to two silicons reacting with water to form hydroxyl groups (-OH) on the surface. This water is covalently bonded to the silica surface and is referred to as chemically absorbed. Water molecules also attach themselves to this surface with weaker hydrogen bonds, referred to as physically absorbed water. This process occurs on the time scale of hours. Above 115°C all physically absorbed water is driven off. At 200°C there are ~ 4.7 -OH groups per nm^2, covering ~59% of the surface. Water in the form of surface hydroxyl leaves the surface at temperatures between 115°C and 600°C. Above 600°C silicon starts to leave the surface along with the hydroxyl groups. At 800°C the surface hydroxyl concentration is down to 11% of the surface area. [Ref. 1.6, Ch. 8] An interesting result mentioned in [Ref 1.6, Ch 8] is the difficulty rehydrating silica which has been in a very dry environment (over P_20_5), at an elevated temperature (from 160°C to 500°C), for an extended period of time (70 hours).

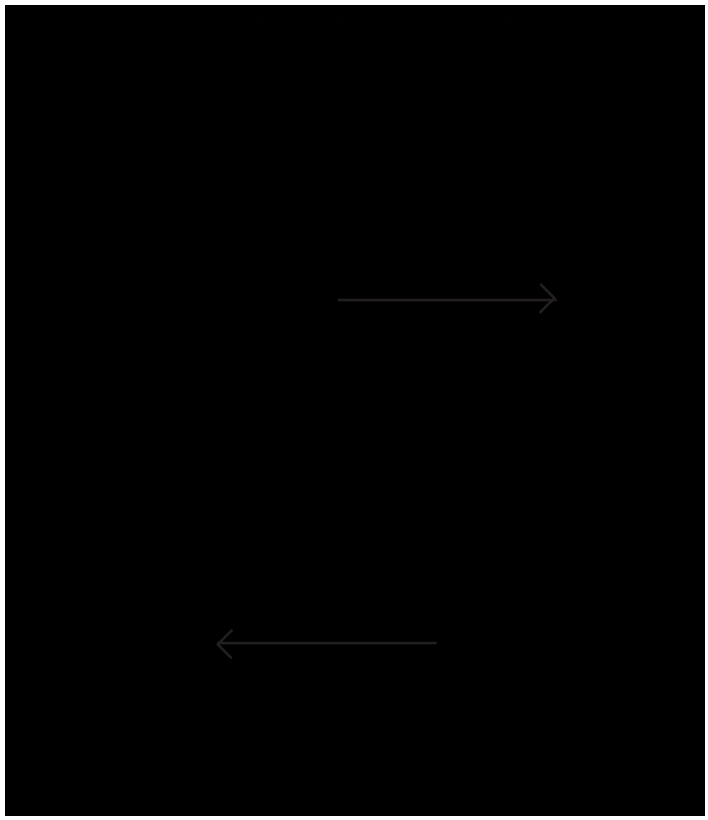

Figure 1.4 Dispersion and absorption curves for water 300-1600 nm. Compiled from Ref. 2

1.5 Effects of water on the surface of silica.

When used for infrared applications silica's above mentioned affinity for water becomes detrimental. For wavelengths longer then visible, waters absorption increases remarkably as illustrated by Fig 1.4 Understanding of the absorption this water layer induces is the focus of this thesis. Ref. 1.7 observed that the surface hydroxyl groups have a single resonance band around 3742-3745 cm-1 using diffuse reflectance FTIR, which is 2671 ± 1 nm. From Ref. 1.2 it is apparent that water has two strong mid infrared resonances located at ~ 2800 and ~5800 nm, with the former being stronger. Overtones of these resonances are the source of the absorption peaks in the near infrared and visible spectrum. The blueshift of the 2700 nm resonance between free and surface water is easily accounted for by the mass effect H-O-H vs Si-O-H. The 5800 nm resonance was not observed in Ref 1.7 and is assumed to be a vibrational mode of H-O-H as opposed to -O-H. It is also interesting to note from Ref 1.7 that exposing the surface to D_2O instead of water produced no change in the reflectance spectra.

Fig 1.5. surface of silica – a chemical picture

Chapter 2

Whispering Gallery Modes of dielectric spheres

2.1 Analytic solutions for fields in a dielectric sphere

Maxwell's equations [Eq 2.1] describe the behavior of electric and magnetic fields in materials characterized by magnetic permeability μ, dielectric permittivity ε, and conductivity σ.

$$\nabla \bullet \mathbf{B} = 0 \qquad \nabla \bullet \mathbf{D} = \rho$$
$$\nabla \times \mathbf{H} - \frac{\partial \mathbf{D}}{\partial t} = \mathbf{J} \quad \nabla \times \mathbf{E} - \frac{\partial \mathbf{B}}{\partial t} = 0$$

Eq. 2.1 Maxwell's Equations. $\boldsymbol{B}=\mu\boldsymbol{H}$, $\boldsymbol{D}=\varepsilon\boldsymbol{E}$, $\boldsymbol{J}=\sigma\boldsymbol{E}$

A finite homogenous material without free charge (ρ=0 everywhere) has solutions to Maxwell's equations in a much simpler form. By applying time and curl derivatives to the above equations, a single partial differential equation (PDE) can be made, which can satisfy either the **E**, **D**, **B** or **H** fields. The vector fields are all satisfied by a single differential equation, expressed here in terms of a generic field **C** [Eq 2.2].

$$\nabla^2 \mathbf{C} - \mu\varepsilon \frac{\partial^2 \mathbf{C}}{\partial t^2} - \mu\sigma \frac{\partial \mathbf{C}}{\partial t} = 0$$

Eq. 2.2 Field in a source free environment.

Separation of variables allows us to treat the time component of this homogenous partial differential equation with ease, finding that it has a dependency of exp(-iωt), where ω is the radial frequency. This allows further simplification of the PDE with the introduction of a new parameter k, $k^2 = \mu\varepsilon\omega^2 + i\mu\sigma\omega$. The problem is now to find the eigenfunctions of the vector Laplacian [Eq 2.3].

$$\nabla^2 \mathbf{C} + k^2 \mathbf{C} = 0$$

Eq 2.3. The vector Laplacian.

A useful approach to solving this vector PDE is to first solve the scalar equivalent problem and then generate acceptable vector solutions from it. The scalar version of this PDE is the well studied Helmholtz wave equation [Eq 2.4]. Consider a solution ψ which satisfies Eq 2.4.

$$\nabla^2 \psi + k^2 \psi = 0$$

Eq 2.4 The Helmholz equation.

Such solutions have been worked out extensively in mathematical textbooks In the spherical basis with radial (r), azimuthal (ϕ), and latitudinal (θ) coordinates the solution takes the form Eq 2.5.

$$\psi = \frac{1}{\sqrt{kr}} Z_l(kr) Y_l^m(\theta,\phi)$$

Eq 2.5. General solution the Helmholtz wave equation in spherical coordinates. [Ref 2.1] Where Z is a Bessel function appropriate for the boundry conditions (Bessel function $J_n(x)$ for finite values at the origin, Neumann function $N_n(x)$ for vanishing at infinity, and Hankel functions for travelling waves). and Y_{lm} is the spherical harmonic.

Given a fixed vector **a** it is then possible to construct three orthogonal vector field solutions **L**, **M**, and **N** [Eq 2.6] which satisfy Eq 2.3. From the nature of their construction several useful vector properties can be identified [Eq 2.7].

$$\mathbf{L} \equiv \nabla\psi \quad \mathbf{M} \equiv \nabla \times (\mathbf{a}\psi) \quad \mathbf{N} \equiv \frac{1}{k}\nabla \times \mathbf{M}$$

Eq. 2.6. Vector solutions to Eq 1.3 Ref. 2.1, Ch 7.1, Eq 5

$$\mathbf{L} \bullet \mathbf{M} = 0$$
$$\nabla \times \mathbf{L} = 0 \quad \nabla \bullet \mathbf{L} = k^2\psi$$
$$\nabla \bullet \mathbf{N} = 0 \quad \nabla \bullet \mathbf{M} = 0$$

Eq. 2.7. Characteristic properties of solutions Eq 2.6. Ref. 2.1, Ch 7.1, Eq 6-9

Bound solutions to these equations, as occur in finite media, are necessarily discrete, so for each characteristic ψ_n, there is $\mathbf{L}_n$, $\mathbf{M}_n$, and $\mathbf{N}_n$ respectively. Since we are interested in solutions which lack free charges, **M** and **N** follow the same behavior as we would expect from the electric and magnetic fields, namely that they "curl" into each other and have zero divergence everywhere. A general linear combination of $\mathbf{M}_n$, and $\mathbf{N}_n$ allows the expression of the electric and magnetic fields without any loss of generality.

$$\mathbf{E} = -\sum_n \left(a_n \mathbf{M}_n + b_n \mathbf{N}_n\right) \quad \mathbf{H} = -\frac{k}{i\omega\mu}\sum_n \left(a_n \mathbf{N}_n + b_n \mathbf{M}_n\right)$$

Eq 2.8. General Electric and Magnetic field solutions. Ref 2.1, Ch 9.22 Eq. 1

It would be convenient to identify any null directional components by application of the properties in Eq 2.7. The direction of the field **M** at any point is perpendicular to the vector **a** and the direction of y 's gradient. Since **a** emanates from the origin, the direction of **M** must necessarily be perpendicular to it. Hence M cannot have a component in the radial direction. Hence if we consider the case where the a_n are zero, **H** consists of only **M** type terms and is therefore polarized perpendicular to the radial direction. In a waveguide or cavity this case is labeled Transverse Magnetic (TM). Similarly if all the b_n terms are zero a similar situation occurs in the electric field and is labeled Transverse Electric (TE).

Eq 2.9a (TE) and b (TM) give explicit expressions for the fields, in a cavity which includes the origin. Solutions for other situations, as described in Eq 2.5, can be found by simple substitution.

$$\mathbf{E}_r = 0 \qquad \mathbf{H}_r = -\frac{n(n+1)}{i\omega\mu_1} Y_{lm}(\theta,\phi)\frac{j_l(k_1 r)}{r} e^{-i\omega t}$$

$$\mathbf{E}_\theta = -\frac{1}{\sin(\theta)}\frac{\partial Y_{lm}(\theta,\phi)}{\partial\phi} j_l(k_1 r) e^{-i\omega t} \qquad \mathbf{H}_\theta = -\frac{1}{i\omega\mu_1}\frac{\partial Y_{lm}(\theta,\phi)}{\partial\theta}\frac{1}{r}\frac{d\left[j_l(k_1 r)k_1 r\right]}{dr} e^{-i\omega t}$$

$$\mathbf{E}_\phi = \frac{\partial Y_{lm}(\theta,\phi)}{\partial\theta} j_l(k_1 r) e^{-i\omega t} \qquad \mathbf{H}_\phi = -\frac{1}{i\omega\mu_1 \sin(\theta)}\frac{\partial Y_{lm}(\theta,\phi)}{\partial\phi}\frac{1}{r}\frac{d\left[j_l(k_1 r)k_1 r\right]}{dr} e^{-i\omega t}$$

Eq. 2.9a TE mode field solutions.

$$\mathbf{E}_r = -l(l+1) Y_{lm}(\theta,\phi)\frac{j_l(k_1 r)}{k_1 r} e^{-i\omega t} \qquad \mathbf{H}_r = 0$$

$$\mathbf{E}_\theta = -\frac{\partial Y_{lm}(\theta,\phi)}{\partial\theta}\frac{1}{k_1 r}\frac{d\left[j_l(k_1 r)k_1 r\right]}{dr} e^{-i\omega t} \qquad \mathbf{H}_\theta = -\frac{k_1}{i\omega\mu_1}\frac{1}{\sin(\theta)}\frac{\partial Y_{lm}(\theta,\phi)}{\partial\phi} j_l(k_1 r) e^{-i\omega t}$$

$$\mathbf{E}_\phi = -\frac{1}{\sin(\theta)}\frac{\partial Y_{lm}(\theta,\phi)}{\partial\phi}\frac{1}{k_1 r}\frac{d\left[j_l(k_1 r)k_1 r\right]}{dr} e^{-i\omega t} \qquad \mathbf{H}_\phi = -\frac{k_1}{i\omega\mu_1}\frac{1}{\sin(\theta)}\frac{\partial Y_{lm}(\theta,\phi)}{\partial\theta} j_l(k_1 r) e^{-i\omega t}$$

Eq. 2.9b TM mode field solutions.

With explicit solutions it is then possible to solve for the resonant frequencies of a dielectric sphere, $\varepsilon=\varepsilon_1$, and radius a, in an infinite dielectric medium $\varepsilon=\varepsilon_2$ by matching of tangential field components at the boundary. This is not difficult to express in spherical coordinates, and produces a transcendental equation, Eq 2.10a for TE and 2.10b for TM, matching Bessel and Neumann functions and their derivatives. Each polarization and mode number l have a different transcendental equation whose roots are a series of unique resonant frequencies. The roots are typically labeled with the index q=1,2,3 … , with q=1 associated with the lowest frequency. For a perfect sphere, the solutions are degenerate in m.

$$\frac{\frac{d}{dr}\left[j_l(k_1 a)k_1 a\right]}{\mu_1 j_l(k_1 a)k_1 a} = \frac{\frac{d}{dr}\left[n_l(k_2 a)k_2 a\right]}{\mu_2 n_l(k_2 a)k_2 a}$$

Eq. 2.10a Transcendental equation for the resonant frequencies of the l^{th} TM mode.

$$\frac{\varepsilon_2}{\varepsilon_1}\frac{\frac{d}{dr}\left[j_l(k_1 a)k_1 a\right]}{j_l(k_1 a)k_1 a} = \frac{\mu_2}{\mu_1}\frac{\frac{d}{dr}\left[n_l(k_2 a)k_2 a\right]}{n_l(k_2 a)k_2 a}$$

Eq. 2.10b Transcendental equation for the resonant frequencies of the l^{th} TE mode.

Whispering gallery modes (WGM) occur near the surface of the sphere in a tight band around the equator. The mode numbers characteristic of this have l ~ m and low q numbers. The number of waves around the circumference of the sphere is roughly l, the latitudinal extent proportional to the difference in l and m, and the depth to which the mode penetrates into the sphere is governed by q.

2.2 Series solutions for resonant frequencies.

$$nx_{l,q} = \nu + 2^{-1/3} A_q \nu^{1/3} + \frac{P}{\left(n^2-1\right)^{1/2}} + \left(\frac{3}{10} 2^{-2/3}\right) A_q^{\,2} \nu^{-1/3} - \frac{2^{-1/3} P\left(n^2 - \frac{2}{3} P^2\right)}{\left(n^2-1\right)^{3/2}} A_q \nu^{-2/3} + O\left(\nu^{-1}\right)$$

Eq 2.11. Series expansion of Eq 2.9 or Eq 2.10, in terms of the size parameter x=ka, the circumference of the sphere measured in vacuum wavelengths, n=l+1/2, A_q, the qth root of the Airy function (see table 2.1), and P, the polarization P=n for TE, P=1/n for TM. Ref 2.3.

Asymptotic series expansions to Eq 2.9 and Eq 2.10 [Eq 2.11] have been given by Ref 2.2, 2.3, 2.4, and 2.5. The first term in this series comes from fitting wavelengths inside the sphere around the equator. The second term comes from the fact that the mode exists slightly inside the surface of the sphere. The greater the q value, the deeper the mode goes into there sphere and the greater an effect this term has. The third term comes from the phase shift that the different polarizations experiences when total internal reflection on the surface of the sphere occurs. Higher order terms are corrections to these effects from the shape of the mode inside the sphere, hence their dependence on polarization, q, and l.

Wavelengths under consideration for practical application range from about 400 nm to 1600 nm and sphere diameters between 50 microns and 2000. Larger, centimeter scale mesosphere were previously investigated by Ref 2.6. Silica has an index of refraction n~ 1.4. Using the first term of Eq 2.11 gives l numbers from about 140 in a small sphere with long wavelength light to 22,000 in a larger sphere with shorter wavelengths. Experiments were performed on spheres ranging from 100 to 1500 microns in diameter at 633, 670, 1319, and 1550 nm, which give l's in the 600 to 20,000 range.

Table 2.2 Roots A_q of the Airy fucntion. [Ref 2.2, Table 1]

q	**A_q**
1	2.338
2	4.088
3	5.521
4	6.787
5	7.944
6	9.023
7	10.040
8	11.009
9	11.936
10	12.829
11	13.692
12	14.528
13	15.341
14	16.133
15	16.906

Table 2.1 illustrates the magnitude of the higher order terms in Eq 2.11. Deeper, higher q number, modes generates a spectra with more variation allowing for easier identification of absolute mode numbers. Ref 2.6 did a spectral fitting for a nearly perfect (< 30 nm deviation) 3.8 cm diameter silica sphere at 1064 nm, confirming the validity of Eq 2.11.

Table 2.1 Term contribution strengths for some different l's, q=1

l	$+^1/_3$ term	Pol TE	Pol TM	$-^1/_3$ term
600	15.65	-1.43	-0.73	0.12
1500	21.24	-1.43	-0.73	0.09
5000	31.73	-1.43	-0.73	0.06
20000	50.37	-1.43	-0.73	0.04

Unlike Ref 2.6, microspheres are normally fabricated with a small eccentricity about their polar axis. For a sphere with such an ecentricity Ref 2.7 estimates the frequency shift by comparing circumference lengths on ellispses tilted by mode precession. The positive shift is for an oblate or flattened spheroid and the negative shift for a stretched spheroid. The ecentricity ε is assumed to be along the z-axis normal to the plane where the WGM's circulate. When l~m in slightly ellipical spheres, this splitting manifests itself as a group of evenly spaced modes [Eq 2.12].

$$\frac{\Delta\omega}{\omega} = \pm\frac{\varepsilon^2\left(l^2 - m^2\right)}{4l^2} \approx \pm\frac{\varepsilon^2(l-m)}{2l}\Bigg|_{l\sim m}$$

Eq. 2.12. Degeneracy lifting of m mode number by axial eccentricy.

2.3 Efficient Coupling to Whispering Gallery Modes

Microsphere morphological resonances were originally studied in the context of Mie scattering off dielectric spheres. Using a scattering theory to deal with cavity phenomena is an activity fraught with some peril, as scattering is a open system type of problem and cavity modes are principally closed systems. For incident plane waves, the strength of the resonance decreases as q does, vanishing at q=1. These modes can be made accessible to plane waves though the use of total internal reflection (TIR).

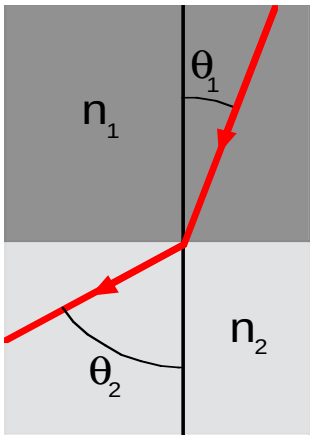

$$n_1 \sin\theta_1 = n_2 \sin\theta_2$$

Fig. 2.1 Snell's Law

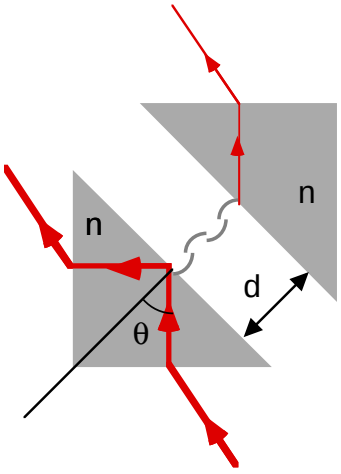

$$n \sin\theta \geq 1$$

Fig 2.2 Frustrated total interal reflection.

Snell's Law [Fig 2.1], describes how light is refracted when passing between media with different indices of refraction. However when a light ray in material 2 exceeds the critical angle $\sin(\theta_c) = 1/n_2$ it cannot propagate though material 1 and instead is totally reflected by the surface. In the first material an exponentially decaying evanescent wave is formed. If a material with an index sufficiently high is close (a few $\lambda/2\pi$), the ray will propagate though the media as if it had been refracted, but (ignoring fixed Fresnel losses from differing indices) with a drop in power $\exp(-2\pi d/\lambda)$ [Fig. 2.2]. This effect allows light which is reflecting off the face of a prism, index $n_p \geq n$ to couple into the otherwise poorly or completely inaccessible whispering gallery modes. Unlike other optical resonators, such as the Fabry Perot cavity, it is possible to vary the coupling by changing the distance between the sphere an the coupler.

Currently there are several different methods of coupling to a microspheres WG modes. The original [Ref 2.8, most others], as described above, is though the total internal reflection of a focused Gaussian beam in prism. The second [Ref 2.9] is through the evanescent wave surrounding a strand of bare single mode optical fiber. The end of a single mode optical fiber can be polished at an angle to effectively create a microscopic prism on it's face [Ref 2.10]. Instead of exploiting TIR, it is also possible to create a diffraction grating on the surface of a sphere though UV holography [Ref 2.11]. Each of these coupling methods has their own unique strengths and pitfalls.

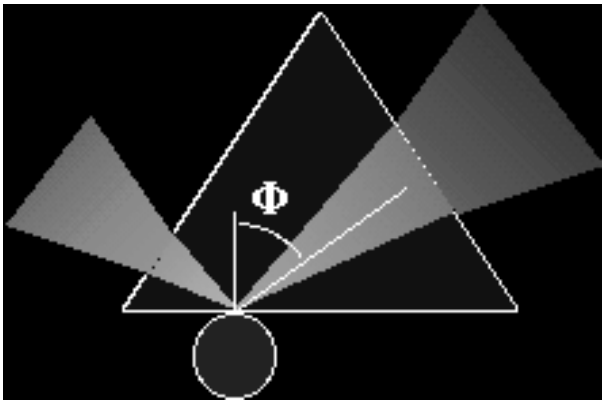

Figure 2.3.a Microsphere coupling to a prism, top view.

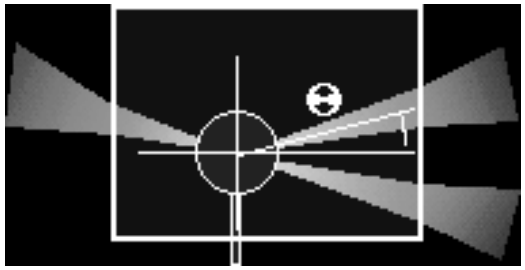

Figure 2.3.b Microsphere coupling to a prism with mode precession, side view.

The frequency and angles of incidence in a prism type coupler determine which mode(s) are excited. Ref. 2.7 provides the definitive investigation of this method. Microspheres excited by a beam not parallel with their equator exhibit a two lobed far field pattern, where the number of nodes equal to l-m. Ref 2.7 demonstrated that these TM/TE $_{lmq}$ modes were equivalent to TM/TE$_{llq}$ modes that are precessing around the axis due to residual nonsphericity. Mode precession is critical to experiments where the depletion of the incident beam is difficult to detect, providing a separate signal of light which has been in the modes. Eq 2.13 and 2.14 give angular requirements and tolerances for coupling to WGM's.

$$\sin\Theta = \frac{\mu}{x n_p} \qquad \sin\Phi = \frac{m}{x n_p \cos\Theta}$$

$$\Delta\Theta^2 = \frac{\sqrt{n^2-1}}{x {n_p}^2 \cos^2\Theta} \qquad \Delta\Phi^2 = \frac{\sqrt{n^2-1}}{x {n_p}^2 \cos^2\Theta \cos^2\Phi}$$

Eq 2.13, Sphere/prism coupling parameters and tolerances. From Ref. 2.7, Eq. 10. Where n_p is the prism index of refraction , angles from Fig 2.4, and $\mu^2=l(l+1) - m^2$.

$$\Theta = \pm \arccos\left(m/l\right)$$

$$\Phi \le \arcsin\left(n/n_p\right)$$

Eq. 2.14. Approximate angles for coupling to WGM's.

2.4. Resonator quality of Whispering Gallery Modes

The quality (Q) of a resonance is governed by the losses associated with it. The spectral width $\Delta\omega$, and relaxation time τ of a resonance with frequency ω are both related to the Q of a resonance [Eq 2.15].

$$Q = \omega\tau = \frac{\omega}{\Delta\omega}$$

Eq 2.15. Resonator Quality or Q.

$$\frac{1}{Q_{observed}} = \frac{1}{Q_0} + \frac{1}{Q_{coupling}}$$

Eq 2.16. Observed resonator quality.

The observed resonator quality is the geometric sum of the qualities of each mechanism [Eq 2.16]. Alternatively, the observed spectral width is the sum of the widths of all the different loss mechanisms. Typically one of these terms predominates over the others. Diffraction losses due to the finite size of the microsphere decrease exponentially and are not relevant to microspheres with D > ~ 20μm. For small prism/sphere separations, losses due to outcoupling of light predominate. The result is the observed Q as a geometric sum of the intrinsic Q_0 and $Q_{coupling}$. Ref 2.7 gives an expression for the Q relating to this loading effect [Eq 2.17]. Increasing the separation decreases the loading due to coupling and allows the measurement of the residual Q_0 with sufficiently large distances. Insufficient decoupling will result in artificially lowered Q_0 measurements

$$Q_{coupling} = \frac{\pi\left(n^2-1\right)\mu m}{2n_p n\cos^2\Theta\cos^2\Phi}\left(1+\frac{\mu^2}{2m^2}\right)e^{-2d/r^*}$$

$$\mu^2 = l(l+1) - m^2 \qquad r^* = \frac{k}{\sqrt{n^2-1}}$$

Eq. 2.17 Resonator Q loading from prism coupling.

Chapter 3

Experimental

3.1 Experimental factors limiting maximum microsphere Q.

A whispering gallery mode in a microsphere is propagating in a real material, which has an intrinsic material attenuation α_{mat} associated with it. By considering the path length of a mode in a microsphere, the material limited Q is $Q_{mat}=kn/\alpha_{mat}$. This intrinsic material loss limit has been reached in Ref 3.1 and nearly so in Ref. 3.2 at visible wavelengths 633 and 670 nm respectively.

$$\delta = \frac{\Delta\nu}{\nu}\frac{n_{ads}^2 - 1}{n_{silica}^2 - 1}\frac{D}{2}$$

Eq. 3.1 Thickness of an adsorbed layer from the frequency shift. Ref 3.1, Eq 4.

Ref 3.1 and 3.2 both observe a drop in microsphere Q, in open air, over the first ~ 2 minutes after fabrication. This is believed to be due to the buildup of a layer of chemically bond water hydrating the surface of the sphere. Ref 3.1 observed the buildup of a δ ~ 0.2 nm thick layer (~ 1.5 monolayers) of water on the surface of a sphere by monitoring the mode frequency shift during adsorption. Ref 3.2 modeled the losses induced by this layer using a mode volume fraction model to get Eq 3.1. Unfortunately this model predicts water limited Q's of ~ $7\text{x}10^{10}$ for D=750 mm at 670 nm, far above what is observed.

$$Q_w \sim \sqrt{\frac{\pi}{8n^3}}\frac{D^{1/2}}{\delta\lambda^{1/2}\alpha_w(\lambda)}$$

Eq 3.2 Water layer limited Q. Ref 3.2, Eq 2

In the smaller spheres, with D< 800mm, it has been proposed [Ref 3.1, 3.2] that surface scattering may be the limiting factor. The effect of surface scattering depends on the subwavelength inhomogeneities on the surface. Irregular surfaces can be treated statistically in terms of the correlation height s and length B between imperfections. In well prepared flat glass s=0.3, B= 3nm [Ref 3.1], while SURF 1997 [Ref 3.2] Atomic Force Microscopy measurements found s=1.7 ± 0.5 nm and B= 5.0 ± 0.5 nm on a microsphere.

$$Q_{ss} \sim \frac{3n^2\left(n^2+2\right)^2}{(4\pi)^3\left(n^2-1\right)^{5/2}}\frac{\lambda^{7/2}D^{1/2}}{\sigma^2B^2}$$

Eq 3.3. Q surface scattering as predicted by Ref 3.2, Eq 1.

$$Q_{ss} \sim \frac{\lambda^2 D}{2\pi^2\sigma^2 B}$$

Eq 3.4. Q surface scattering as predicted by Ref 3.1, Eq 2.

Ref 3.1 and Ref 3.3 propose that the losses observed in silica fibers from bulk Raleigh scattering may be suppressed in microspheres by the limited number of free space and cavity modes accessible to a scatterer. Scatterers in a silica fiber can couple to a free space mode in almost any direction, forward and backscattering into the mode representing a very small fraction of the possible radiative modes. However in a high Q microsphere, the number of radiative free space modes is limited by total internal reflection at the sphere's surface, leaving only the forward and back propagating modes as allowable inside the sphere. Ref. 4.3 estimates that bulk scattering could be suppressed, and conversely the Q enhanced, by a factor of up to 2.8 for TE and 9.6 for TM modes.

The phenomena of mode splitting lends experimental weight towards the possibility of bulk scattering loss suppression. Observed at both optical [High Q, Ref. 3.2, 3.4] and microwave frequencies [Low Q, Ref. 3.5], mode splitting occurs when the losses due to scattering into the counter propagating mode approach the looses from other sources. The coupling splits the frequency degeneracy of the two modes, creating a closely spaced doublet. While it is possible that coupling between modes could occur from non linear processes, Ref 3.4 discounted this due to the lack of change in the splitting width over two decades of intensity. The resonance splitting observed matches a weakly coupled oscillator model. This splitting also manifests as a beat note the transient regime. A Fourier transform of the decaying signal gives the corresponding spectra [Ref 3.4], analogous to FTIR and FT-NMR spectroscopy techniques.

Mode splitting is expected to be confined to the very low effective volume l=m, q=1 whispering gallery modes. The scattering the splitting can come from either surface scatterers or from internal Raleigh scatters. Ref 3.3 predicts that at 633 nm, internal scattering predominates in spheres larger then ~ 40mm.

$$V_{eff} = 3.4\pi^{3/2}\left(\frac{\lambda}{2\pi n}\right)^3 l^{11/6}\sqrt{l-m+1} \approx 3.4\pi^{3/2}\left.\frac{a^2\lambda}{2\pi n}\right|_{l\sim m>>1}$$

Eq 3.5, Effective volume for q=1 modes. Ref 2.8, Eq. 4

$$\left(\frac{\Delta\omega}{\omega}\right)_{is} \approx \sqrt{\frac{3\lambda^4\alpha_{is}}{8\pi^3 n^4 V_{eff}}}$$

Eq. 3.6. Predicted splitting from internal scattering, q=1 modes, Ref 3.3 Eq 34.

$$\left(\frac{\Delta\omega}{\omega}\right)_{ss} \approx \frac{3.7\sigma B}{\lambda^{1/4} D^{7/4}} \qquad \left(\frac{\Delta\omega}{\omega}\right)_{is} \approx \frac{7.5\times10^{-7}\mu m^{3/2}}{\lambda^{11/12} D^{7/12}}$$

a *b*

Eq 3.7, Predicted splitting from surface scattering (a) and internal scattering (b). For an TE l=m, q=1 mode. Ref 3.3, Eq 34 and 39.

3.2 Microsphere Fabrication Techniques

To obtain whispering gallery mode resonances are near the intrinsic absorption limit, silica spheres are fabricated from extremely clean, smooth silica rods using an oxy hydrogen microtorch. Silica which does not meet these requirements will not form microspheres with very high Q's. In the ultraviolet regime metallic impurities degrade the transmittance while in the infrared water is the principal contaminate. Interest in silica for fiber optic communication has lead to industrial production of very high quality (<5 ppm –OH), very low absorption silica stock. Rods of this type of synthetic fused silica are the best known for microsphere production.

Rods with diameters varying from 1.2 to 6 mm have been successful in the fabrication of high Q microspheres. Large rods are hard to work with, requiring an additional torch setup to produce the heat necessary to draw them down to a working diameter of ~ 1mm. Smaller rods break easily and are diffusion of atmospheric water can contaminate them over months of storage in a moist environment. Surface water diffusion is also a problem with larger rods. However they are thick enough to allow etching away the problem layer of silica with concentrated HF acid.

In addition to water absorption the quality of the silica surface also affects the obtainable Q. Dirt, grease, and dust collect on any exposed surface and must be removed. The easiest way is by scrubbing the surface with a commerical non-abrasive glassware detergent such as Alconox. A wet test tube cleaner coated with Alconox is effective for scrubbing, as long as care is taken not to scratch the silica with any supporting metal protrusions. An easy way to monitor the progress of cleaning is by heating the end of the dried rod till it glows white hot. This launches light down the rod, illuminating any defects. Color figures 3.1a and 3.1b illustrate such a test on clean and an uncleaned rods. The clean silica is dark with the exception of a portion on top where the shape changes because the rod was hand pulled from a thicker chunk. On the dirty rod there are many bright surface scattering centers, orange-yellow contaminant scars, as well as a diffuse film of water heated off by the flame. This diffuse water film is also observed on clean silica rods which have not been stored in a dry environment.

After scrubbing the sphere it is often beneficial to dip it in fuming nitric acid for 10-30 minutes to chemically remove any grease or other chemicals bonded to the silica surface. Fuming sulfuric and hydrochloric acid have also been used, but neither has the additional oxidizing power of nitric acid. The final step in preparing the silica is to use a 50% HF solution to etch away the outer layer of the silica which may have become contaminated by water. Depending on the history of the rod you may need to etch away from 1.5 mm to none at all. An HF etch will smooth down smaller surface deflects, but larger defects and dirty areas will produce irregular results. As mentioned before, heating the end of the rod white hot will indicate if this is a problem.

An oxy-hydrogen microtorch is used to fabricate the microspheres from the silica stock rod. Hydrogen and oxygen are premixed with a jewelers' microtorch, bubbled through a water/ethanol solution, and then fed through a modified syringe with a metal needle. Electrolysis of water and gas tanks are the two sources of hydrogen and oxygen which have been used in successful record Q measurements [Ref. 3.1 and 3.2]. It is strongly recommended for safety reasons that if bottles of compressed gas are used that flame stops be installed on the lines leading from them. The microtorch system is homebuilt and hence has a much greater risk of unexpected failure or behavior then a prepackaged

system. The mixed gas is bubbled through an ethanol/water solution, equal amounts by volume, to improve the performance of the flame. This smooths out any irregularities in gas flow and slightly cools the flame, making it more uniform and easier to work with. A 40 ml solution will "wear out" after several hours of use. It is recommended for safety reasons that the container have an emergency pressure release and be non flammable.

The syringe body should be filled with a large amount of copper mesh. The large heat capacity and high thermal conductivity act to quench any flame burning back into the system. Tips are standard, flat cut needles with an inner diameter between about 250 and 750 microns. Spheres about twice the aperature size can be easily fabricated up to diameters around 1300 microns. Beyond this size the large mass of the silica makes the spheres act "heavy" in the flame, insufficiently pushed up by the gas flow, increasing the difficulty of good fabrication. Accounting for this difficulty, spheres with diameters of up to 2000 microns have been fabricated. However they have less then perfect shapes, as can be observed by visual inspection.

A good working flame has a crisp pale blue cone which is not bowed inward or outward. Hydrogen and oxygen burn nearly clear, so having a black background or a darkened room make working with the flame easier. An outward bowed flame is lighter in color, does not have enough oxygen, and hence is too cold. This silica will not heat up quickly and have a tendency to solidify quickly when not in the hottest part of the flame. An inward bowed flame is too hot, and dark blue or purple in color. This flame has a very strong temperature gradient, making it hard to heat the entire sphere uniformly. This type of flame is also at risk for collapsing and flashing back though the system. After the flame is first started, dust particles can been seen burning up in the flame as orange flashes. After 5-10 minutes the frequency of flashes drops. If the flame is in a mostly enclosed volume, such as an unsealed drybox, about 15 minutes of burning will remove almost all of the dust in the box.

Surface tension can be exploited to form spherical and nearly spherical fluid objects, because it minimizes surface area. Raindrops exhibit this as their primary shape determiner, as does orange juice floating in space. Microspheres are formed by drawing out a length of thin silica with a thicker portion at the end. Heating the thicker end causes it to ball up. The upward pressure from a flame gasses allows the thin stem to be bent, positioning the axis of sphere perpendicular to the supporting rod. A faster and more advanced technique exploits the combustion edge in the center of the flame cone, holding the sphere in the hottest part of the flame while keeping the stem in the cool precombustion area. After the sphere is formed on the end of stem, it then can be brought back closer to the flame for finishing. This allows adjustment in the orientation of the sphere's stem and the mode precession axis. Mode precession creates a separated outcoupled beam which can be spatially separate from the incoupled beam, allowing for measurement of light which has been exclusively in the mode. At this point the sphere should be glowing white hot but not changing shape. Slowly removing the sphere from the hot region near the flame over the course of several seconds allows it to anneal. Annealing lowers the glassificiation temperature T_g, and hence reduces the density variations in the silica. Annealing also allows time for small surface variations to be smoothed out by surface tension. Commercial glass manufacturers are very concerned with how homogenous their glass melt is and sometimes anneal their wares over the course of days.

To extend this fabrication technology to larger spheres, it might be possible to use commercially manufactured silica spheres, attach them to the end of a silica stem and then nitric acid drip, HF etch, and anneal them, retaining the bulk shape but improving the surface quality.

3.3 Apparatus and measurement methods

Three different laser sources were used in this thesis, two of them successfully and one whose was deemed impractical. The first two systems used the same external diffraction grating stabilized laser diode system based on Ref 3.6, 3.7, 3.8, and modified by J. Buck. Laser diodes are tunable by changing current, temperature or through optical feedback. A grating the Littrow configuration, with the first order diffraction peak aligned with the incident beam provides a convenient way to stabilize the frequency of a laser diode. By diffracting ~10% of the incident light back into the laser diode, a stable MHz or sub MHz linewidth can be achieved. Turning the grating coarsely adjusts the frequency, while a piezo can tune the cavity length to provide fine scanning. This technique is limited by quality of the cavity which can be formed between the diffraction grating and the laser diode. Fresnel reflections from collimating optics, diode packaging, and the diode face can degrade the cavity. Current tuning in AlGaAs lasers typically is ~ 3MHz/mA for freerunning lasers and ~300kHz/mA for those dominated by optical feedback [Ref 3.7].

Changing the operating temperature of an AlGaInP 633 nm red laser diode will tune it by ~ 0.2 nm/°C, alternately 150 GHz/°C. To control this property the laser diode sits in a two stage thermoelectricity cooled temperature servo controller which provides mK level stability. The first stage was directly driven from a power supply to provide sufficient cooling power to change the free running wavelength of the laser diodes. With the 10 mW, 635 nm diodes it was hoped that it would be possible to temperature tune them down to ~633 nm and reference them against a stable HeNe laser to provide an absolute frequency measurement. However, all diodes purchased had room temperature (23°C) free running wavelengths of 640 +/- 2 nm. While a 2 nm/10°C temperature tuning is practical, the wavelength differences measured would have forced the temperature of the laser to near or below freezing at which point water condensation starts shorting out the circuitry.

Due to this difficulty, a 30 mW, 675 nm Phillips model CQL806/30D laser diode was substituted into the setup, with a corresponding change in diffraction grating. To improve the throughput of the system, laser diode was temperature tuned from a room temperature operating wavelength of 676 nm to 674 nm to improve the signal performance of the 670 nm linefilter protected photo multiplier tube (PMT). The experiments at JPL were carried out in a lit, shared laboratory which precluded blacking out the room as had been done previously at Caltech. The beam was shaped using an anamorphic prism pair and isolated with an Optics For Research IO-670-2 free space isolator. A switched signal with a ~ 50 ns fall time was created using an NEC Acousto-optic modulator. This limited ringdown measurements to Q's greater then ~ 2×10^8. The beam was then launched into a single mode optical fiber. Of the 23 mW measured off the grating, 4 mW successfully couples into the fiber. Residual backreflections not fully isolated by the OFR isolator, broaden the laser linewidth to ~ 3 MHz, and the spectrally measurable Q to < 10^8. The laser diode is tunable over ~ 3.9 GHz without mode hopping. The gap between spectral and ringdown Q measurement ranges was not important as low Q modes at 670 nm were not of interest to this project.

A high power, fiber coupled Lightwave Electronics ILX series 125 1319 nm diode laser pumped Nd:YAG laser provided an excellent source for making Q measurements in the infrared. This laser provided ~ 60 mW of power with a linewidth < 15 kHz. Unfortunately the laser was only piezo tunable over ~ 100 MHz. Temperature tuning extended the scanable range by several GHz, but with

a response time in seconds. A homemade fiber ring cavity with FSR=55.8 MHz, measured by sideband modulation, and finesse ~ 20 provided a reference standard for spectra taken at this wavelength. Even with an internal 30 dB optical isolator, an additional optics for research 30 dB isolator needed to be added to prevent feedback from the microsphere from affecting laser performance.

The coupling prism used was a 60-60-60 triangle prism made of SF-18 glass, n=1.648, which by Eq 2.14 gives an idea coupling angle of Φ=61.2°. The beam was launched normal to the prism face (Φ ~ 60°) to ensure that chromatic dispersion did not affect alignment strongly. Exploiting mode precession to obtain a clean signal from the mode, the beam was typically launched Θ ~ 15° off the sphere's polar axis. Light was launched into the coupling prism by a symmetric pair of aspheric lenes in front of a single mode fiber. This allowed the operating wavelength to be changed without disturbing the alignment. Far field emission patterns from the coupler were focused with a lens into a 1mm diameter flexible fiber light pipe which lead to the appropriate detector. This also allowed detectors to be switched without disturbing the alignment.

The microsphere was mounted on a steel square, 1"x1"x .25", that clung to a kitchen magnet on a Burleigh model PZS-100 piezo Microstage. With an observed travel of 54 microns over 100 Volts, a 200 mV change would shift the microsphere by 670/2π nm, reducing the coupling by ~ e^{-2} or 13.5%, Eq 3.6. Typically the microsphere was decoupled 1-2 Volts from the face of the prism to obtain an unloaded resonator Q. The microstage was attached to a XYZ micrometer adjustable stage for coarse positioning.

A Thorlabs DET 410 InGaAs photodiode was used for detection at 1319 nm. InGaAs is also responsive at 670 nm so it was possible to use the red light to monitor decoupling without switching detectors. The DET 410 has a response time of 5 ns into a 50 Ω load. Since the scan frequency was 50Hz and digital captures of spectra consisted of 2500 points, a response time of ~ 8 μsec was required. By replacing the 50 Ω internal load resistor with a 100kΩ resistor the signal voltage was increased by 2000 without affected the response.

Measurements at 670 nm were performed with a Hamamasu R928 photo multiplier tube. Biased at ~1000V to provide ~60 dB gain on a photocathode responsivity of 35 mA/Watt. A rise time of ~ 2 ns far exceeded the bandwidth necessary. To protect this highly sensitivity detector from accidental burn out due to ambient light, a Newport 10LF10-670, 10 nm FWHM centered at 670 nm line filter was mounted in front of it.

A typical experimental procedure involved three stages; fabrication, finding the modes, and then fine tuning and decoupling. Microsphere fabrication techniques have been previously mentioned. After fabrication, the mounted microsphere was placed on the Burleigh stage and positioned within ~5 mm the face of the coupling prism using the XYZ stage control and a 50x binocular microscope. Illumination of a white target underneath the microsphere provided a high contrast shadow image of the sphere. At these distances and angles, a reflected image of the sphere is visible in the prism, effectively doubling the resolvable distance between the prism and the sphere. This final few micro distance is then closed by the piezo microstage. The focused beam spot is roughly aligned with the microsphere using a small 45-45-90 observation prism. Even on a clean prism face, a tightly focused beam will scatter some light allowing it's location to be determined. The tighter the focus, the brighter and sharper the spot. For non contact coupling, critical in obtaining high Q's at 670 nm

(633, 780, 850 nm too see Ref 3.1, 3.2), the sphere is gradually brought closer to the prism while the position of the spot is scanned over the position of the sphere, until faint flashes of modes are seen. Scanning at ~ 1 Hz makes the individual modes flashing resolvable to the eye. An iris and lens focus the mode light into the previously mentioned fiber light pipe where it is sent to a detector. The sphere is then retracted from the prism and the optical alignment tweaked to improve the signal. A paper box is then placed around the entire setup in order to minimize shifts in the resonances due to eddy currents in the air.

To measure the Q at 1319 nm, a screen shot is taken of the spectra. In order to measure the Q at 670 nm, the oscilliscope must be set to trigger on a peak as it is scanned. This trigger then quickly (< 100 ns) extinguishes the light, and a second fast oscilliscope can be used to capture the ringdown.

3.4 Measurements and observations

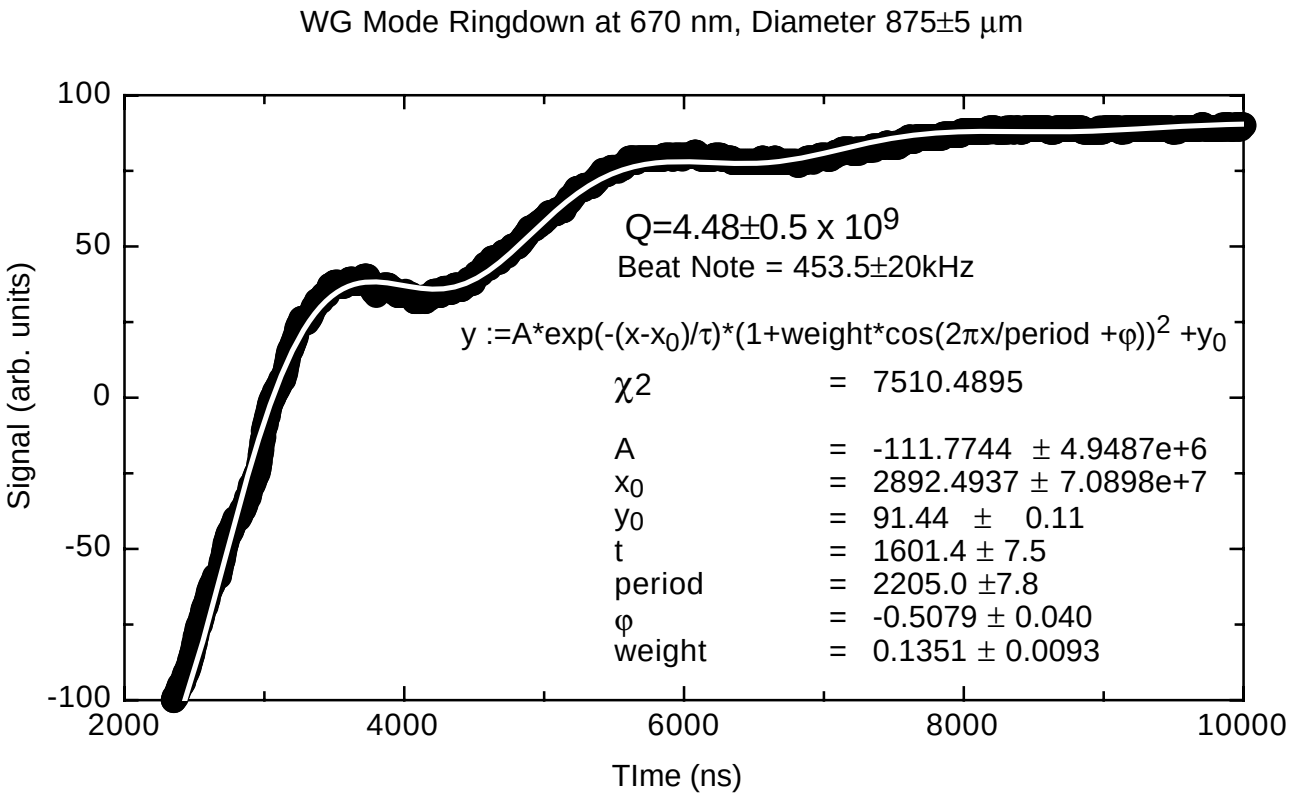

Figure 3.4 Rindown response of a High Q mode at 670 nm . Note beating component indicating mode splitting. Measurement made < 2 minutes after fabrication.

Microspheres were fabricated as previous described, coupled to, and their Q's measured at 670 nm, 1319 nm, or both. Contact with the prism had a marked impact on the Q at 670 nm, dropping it to ~ $2x10^9$, no such effect was noticed at 1319 nm. In addition, Q's measured within ~ 2 minutes of fabrication had notably higher Q's, often displaying a weak beat note indicating that the losses were low enough and scattering high enough to create a partial backscatter mode splitting [Fig 3.4]. Quickly measuring the Q at 1319 nm is difficult due to the limited fast scan range of the Nd: YAG,

and the difficulties associated with switching to an invisible wavelength. Theses difficulties are relieved somewhat by the use of fiber optics, although The two points above the trend in figure 6.5 both happened to be spheres where the red and infrared coupling were nicely aligned on top of each other, eliminating the need to tweak the optics and hence reducing the time to make the measure. As Ref 3.9 did at 780 nm, a thermal bistability was observed at 1319 nm, as shown in Fig 3.5.b. These bistabilites increased with decreasing sphere size. Thermally bistable modes exhibited a tendency to "stick" to the laser frequency, sometimes being pulled several GHz from their natural resonant frequency . This effect was useful in finding resonances in smaller spheres with very low mode spectral density. In the smallest sphere only 4 modes were present over the entire tuning range of the laser, of these three exhibited a very pronounced thermally bistablity. Thermal bistability's adverse effect on mode posistion precludes frequency shift measurements of the adsorbed monolayer as was done in Ref 3.1.

An attempt was made to treat a sphere with Sigma Cote, a commercial organo silane based water repellent glass coating. Due to the hazardous nature of Sigma Cote the treatment was done in a fume hood. The sphere showed $Q<10^8$ at 670 nm and under visible inspection dust particles adhered to the surface. A procedure for treating spheres without dust contamination needs to be developed.

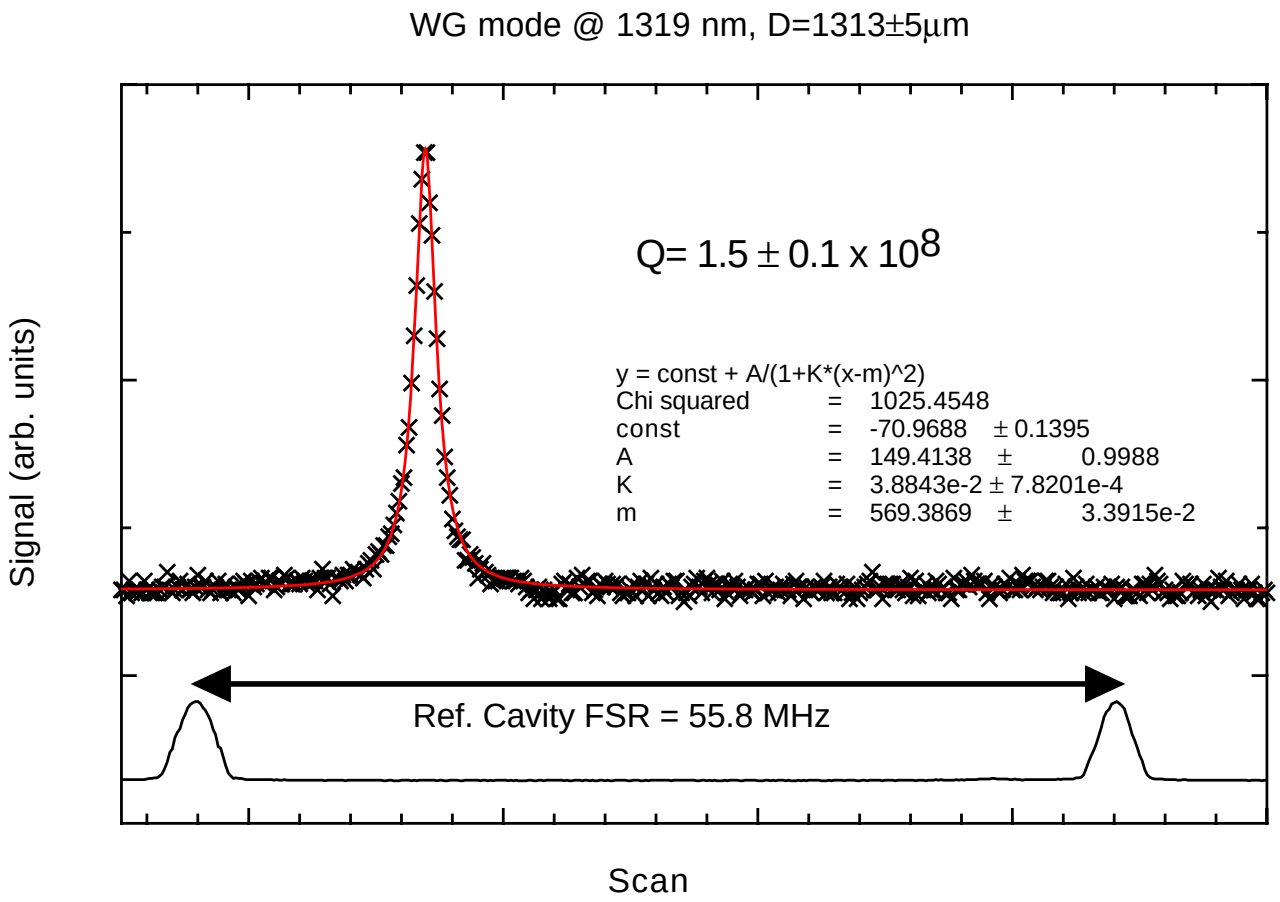

Fig 3.5.a. Typical spectra at 1319 nm not showing thermal bistability.
Upscan and downscan (not featured) both have a Lorentzian. response.

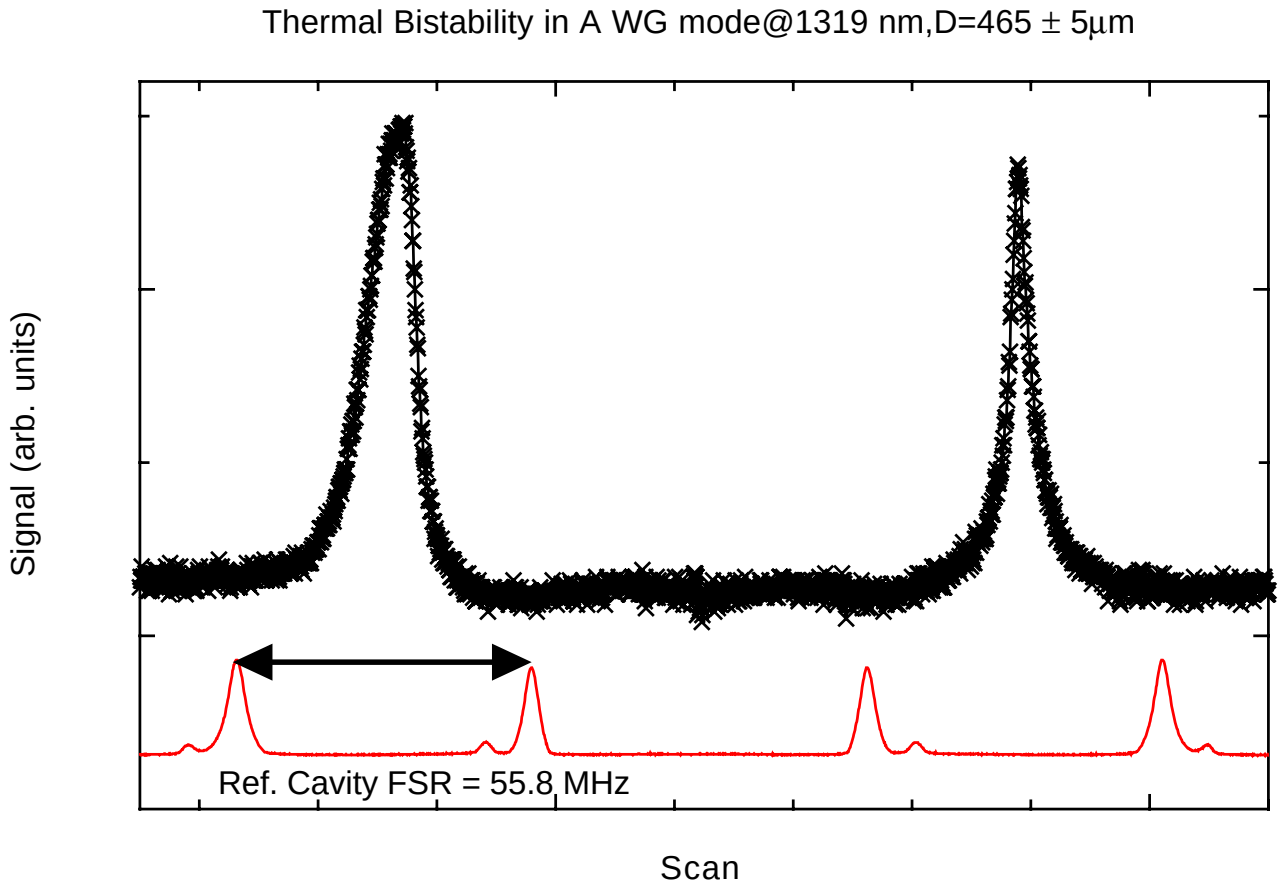

Figure 3.5.b. Spectra of a mode at 1319 nm exhibiting a thermal bistability.
Note the asymmetric, non Lorentzian shape of the individual peaks as well as the disparity between the two.

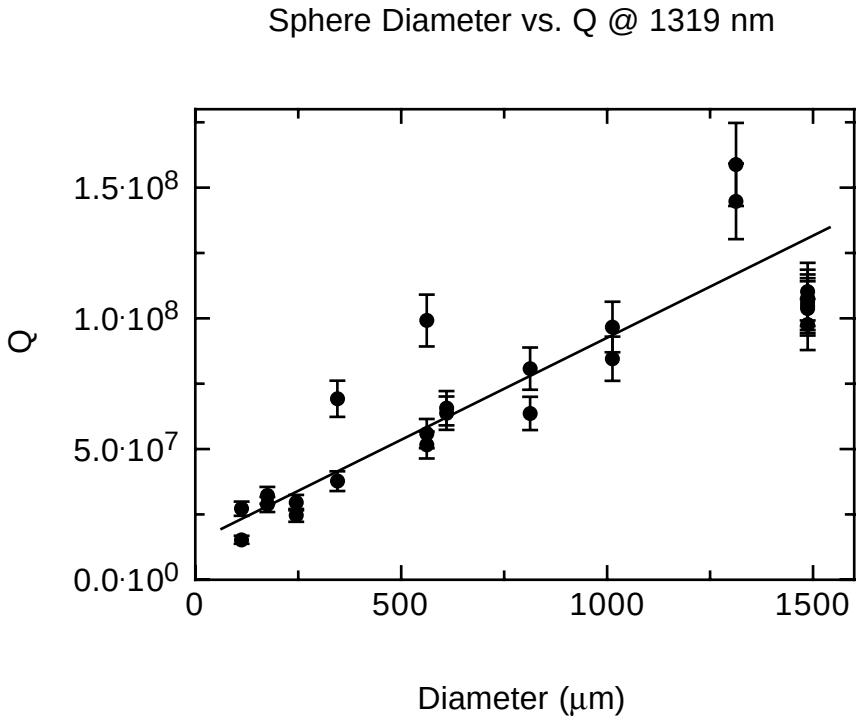

Fig 3.6. Observed Q vsDiameter for select spheres.

A series of microspheres with diameters from 100 μm to 1500 μm had their Q measured as quickly as possible after fabrication [Fig. 3.6]. On several occations coupling at 1319 nm was achieved quickly and the Q measured within ~1.5 - 2 minutes rather then the typical ~ 3-4 minutes. In those spheres Q's above the trend line were observed. Beyond 1300 μm appears to be where fabrication limits inhibit the Q. For those spheres not measured quickly and not too large, the trend in Q appears to be linear in diameter.

3.5 Discussion

Ref 3.1's formula for frequency shift [Eq 3.1] due to the adsorption of a thin layer ($\delta << \lambda/2\pi$) on the surface of a sphere can be used to determine the increase in attenuation coeff a by evaluating it for the case of complex valued indices of refraction. From Ref 3.10 Eq 7.53 the complex wavevector can be expressed in terms of propagation and attenuation terms $k = \beta + i\,\alpha/2$, where the intensity drops as $\exp(-\alpha z)$. From the optical properties of silica and water listed in Table 1.2 it is evident that the loss per wavelength is very small so $\beta >> \alpha$. It is also evident that $\alpha_{water} >> \alpha_{silica}$. Hence consideration of only the complex index of refraction of water is necessary. Ref 3.10, Eq 7.55 gives $\alpha \approx \beta\, \mathrm{Im}(\varepsilon)/\mathrm{Re}(\varepsilon)$ under these conditions, which can be rewritten $\mathrm{Im}(n^2)=\mathrm{Im}(\varepsilon) \approx n^2\alpha/k$ by assuming $\mathrm{Re}(\varepsilon)\approx\varepsilon\approx n^2$ and $k \approx \beta$.
Taking the imaginary part of the change in the wavevector k allows us to compute a new effective

$$\frac{\alpha_{eff}}{2} = \mathrm{Im}(\Delta k) = \mathrm{Im}\left(k \frac{2\delta}{D} \frac{n_{silica}^2 - 1}{n_{ads}^2 - 1} \right) \approx \frac{2\delta}{D} \left(n_{silica}^2 - 1 \right) \frac{n_{ads}^2 \alpha_{ads}}{\left(n_{ads}^2 - 1 \right)^2}$$

Figure 3.9. Effective attenuation from a thin layer.

attenuation coefficient, approximating the imaginary component of water's dielectric constant as a small perturbation on the system. Applying this to the attenuation limited Q formula $Q_{abs} = kn/\alpha$ gives an equation for how the Q should be limited by the water layer. The functional dependence of this result on D and wavelenght is the different then Eq 3.2, which used a fractional mode volume approach [Ref. 3.2 Eq 2].

$$Q_W = \frac{\pi D}{2\delta\lambda\alpha_W(\lambda)} \frac{n_{silica}}{\left(n_{silica}^2 - 1 \right)} \frac{\left(n_{ads}^2 - 1 \right)^2}{n_{ads}^2}$$

Fig. 3.10. Proposed water limited Q formula.

For D=750mm, λ=670 nm, δ~0.2 Eq 3.8 gives $Q_w \sim 7\text{x}10^{10}$, which is much higher then the observed Q's which are believed to be water limited. Similarly, Eq 3.10 predicts an unreasonably high $Q_w \sim 1.2\text{x}10^{13}$. At λ=1319 nm, the Ref 3.2 model give $Qw \sim 1.2\text{x}10^{8}$, which is similar to the observed values, but the diameter dependence does not appear to match the trend particularly well. Both of these models don't agree with measurements made at 670 nm and 1319 nm. While evidence from Ref 3.1 and 3.2 strongly suggest the presence of a water layer, and that it reduces the Q to $\sim 10^9$ at 670 and 10^8 at 1319 nm what is not clear is why the drop in Q is only about an order of magnitude while the increase in free water's

aborption is ~2.5 orders of magnitude [Table 1.2]. Ref. 1.7 gives evidence that one of the infrared absorptions due to vibrational modes is no longer present, but from inspection of dispersion curves in Ref 1.2 it does not appear to be a particularly broad resonance. If the water layer is chemically adsorbed on the surface, it would have lost several degrees of freedom and their associated resonances. If a chemically adsorbed water on the silica surface absorption curve could be determined, the validity of Eq 3.10 could be checked in a more rigorous fashion.

Comparison with Ref 3.4's D=3.8 cm sphere at 1064 nm provides no useful information towards the issue of water absorption, as their sphere appears to be probably scattering limited. The material limited Q at 1064 nm is 4.8×10^{10} for dry silica, far below the observed 9.4×10^{7}. Since higher water dependent Q's in smaller spheres were observed, and the attenuation of water is lower at 1064 nm then 1319 nm, it's reasonable only to assume that this experiment was not water limited. No thermal bistability was observed, but that does not necessarily rule out absorption losses as no power levels or coupling efficiencies were quoted, and the silica quality is unknown. While the sphere's deviation from perfect was quoted as < 27 nm, the subwavelength surface is of unknown quality. Assuming it's rougher then a microsphere the surface scattering formulas give a range of 1.9×10^{7} to 1.5×10^{11}, indicating that surface scattering is a possible loss mechanism. No specific mention of not touching the prism to the face of the sphere adds contact scattering losses as a possible mechanism limiting the Q.

Since the observed Q's at 1319 nm were independent of if the sphere touched the surface or not, and many of the modes exhibited thermal bistability it is reasonable to assume that $Q_{ss} > 10^{8}$ at 1319 nm. Both models of surface scattering predicted Q's far in excess of what was observed. In a 100mm sphere with surface roughness observed in Ref 3.2 were 6.1×10^{8} [Ref. 3.1] and 1.52×10^{10} [Ref 3.2].

While in the red and near infrared [Ref 3.2], surface scattering may be a limiting factor, it is very doubtful that it is the barrier to observing substantially higher Q's at 1319 nm. Predictions of Q_{ss} at 1319nm range from 4 to 11 times greater then scattering limited Q's at 670 nm. This does however potentially limit the Q to below that from the bulk material losses.

Conclusion

The factors limiting the resonator quality (Q) of whispering gallery modes in silica microspheres have been identified as water adsorption on the surface, surface scattering, and material attenuation. Models these phenomena have been proposed in the literature and in this work.

Microsphere whispering gallery mode Q's of ~10^8 observed at 1319 nm, far from the material limit of ~10^{11}. This independent evidence further supports the theory of chemical adsorption of a monolayer of water as limiting the Q in the infrared. A model describing the Q as limited by this layer was developed and it's linear dependence on diameter agrees with experimental data to date.

Understanding of factors limiting microsphere Q's would benefit from further experimentation in several areas. Drybox work would extend the timescales under which the water layer is believed to be formed. Coating experiments with liquids in a dust free environment or HF vapor could provide hydrophobic microspheres which retained their high Q for longer periods of time. With the fiber optic coupling setup it is easy to introduce a variety of wavelengths without modifying the basic coupling setup. Along these lines, measurements at 1064 nm or 1550 nm would provide more information on water absorption. Investigation at visible wavelengths shorter then 633 nm, such as provided by a Ar+ or frequency multiplied Nd:YAG laser would be useful in determining the role of scattering in microspheres.

Acknowledgments

I would like to thank H. Jeff Kimble, Vladimir S. Ilchenko, Lute Maleki of JPL's Frequency Standards Laboratory, Wren Montgomery, and Allison Roberts. This would not have been possible without them.

I would also like to thank Dave Vernooy, Joseph, Buck, Jason McKeever, Caltech SURF Program, Caltech Physics Department, Rabi Wang, and X. Steve Yao for their assistance.

Funding for SURF 1997, SURF 1998, and Senior Thesis was provided by The Ritcher Foundation, The Nickerson family, and the Office of Naval Research. Work performed with NASA's Jet Propulsion Laboratory and the Caltech Quantum Optics Group.

This document was written in Microsoft Word, figures created in ClarisWorks, graphs in Pro-Fit, and assembled with Adobe Pagemaker 6.0.

References

1.1 “Fundemental optical attenuation limits in the liquid and glassy state with application to fiber optic waveguide materials.” by D. A. Pinnow, T. C. Rich, F. W. Ostermayer, Jr., M. DiDomenico, Jr. in Applied Physics Letters. Vol 22, No. 10 on 15 May 1973.

1.2 “Optical constant of water in the 200 nm to 200 mm wavelength region.” George M. Hale and Marvin R. Querry. Applied Optics, Vol 12, No. 3. March 1973

1.3 Synthetic Fused Silica. Melles Groit 1998-99 Catalog.

1.4 Schott Guide to Glass. Heinz G. Pfaender 1983

1.5 “Ultimate low loss single mode fiber at 1.55 mm”, Miya, T., T. Terunuma, T. Hosaka, and T. Miyashita, Electron. Lett. 15:106 (1979)

1.6 “The Colliod chemistry of silica and silicates” by Ralph K. Iler, 1955, Cornell University Press.

1.7 “Detection of surface hydroxyl species on quartz , gamma alumnina, and feldspars using diffuse reflectance infrared spectroscopy.” C. M. Koretsky, D. A. Sverjensky, J. W. Salisbury, and D. M. D’Aria in Geochimica et Cosmochimica Acta, Vol 61, Np 11 pp 2193-2210 1997.

2.1 “Electromagnetic Theory”, Julius A. Stratton, McGraw-Hill, 1941

2.2 “Resonance structure of Mie scattering: distance between resonances”, by Petr Ch´ylek, JOSA A Vol 7m No 9, Sept 1990 p.1609-1613

2.3 “Asymtptotic formulas for the positions, widths, and strengths of resonances in Mie scattering”, JOSA B, Vol9, No 9, Sept 1992, p 1585-1592 by C. C. lam, P. T. Leung, K. Young.

2.4 “Asymptotic expansion of morphological resonace frequencies in Mie scattering” by S. Schiller in Applied optics Vol 32, No 12, 20 April 1993.

2.5 “Resonance component of backscattering by large dielectric spheres” J. R. Probert-Jones, JOSA A Vol 1, No 8, August 1984.

2.6 “High resolution spectroscopy of whispering gallery modes in large dielectric spheres”, Stephan Schiller and R. L. Byer. Optics Letters Vol 16, No 15 August 1, 1991 p 1138-1140.

2.7 “High- Q optical whispering gallery microresonators: precession approach for spherical mode analysis and emission patterns with prism couplers”, M. L. Gorodetsky, V. S. Ilchenko, Optics communications 15 December 1994 113 (1994) p133-143

2.8 “Quality factor and non linear properties of optical whispering gallery modes”, V.B. Braginsky, M. L. Gorodetsky, and V. S. Ilchenko, Phys Letters A, 29 May 1989 Vol 137, No. 7.8.

2.9 “Excitation of resonances of microspheres on an optical fiber” A. Serpenguzel and S. Arnold and G. Griffle, Optics Letters Vol 20, No 7 , April 1, 1995.

2.10 “Pigtailing the high-Q microsphere cavity: A simple fiber coupler for optical whispering-gallery modes”, by V.S.Ilchenko, X.S.Yao, L.Maleki in Optics Letters, 1999 (in press) scheduled for June 1 issue.

2.11 “Coupling light from a high-Q microsphere resonator using a UV-induced surface grating”, V.S.Ilchenko, D.S.Starodubov, M.L.Gorodetsky, L.Maleki, J.Feinberg, (to be) CTuC4 presented at CLEO/QELS, Baltimore, May 23-28, 1999

3.1 “Ultimate Q of optical microsphere resonators”, M.L. Gorodetsky, A. A> Savchenkiv, and V. S. Ilchenko Optics Letters April 1, 1996 Vol 21, No.7.

3.2 “High-Q measurements of fused silica microspheres in the near infrared” by D. W. Vernooy, V. S. Ilchenko, H. Mabuchi, E. W. Streed, and H. J. Kimble. Feb 15, 1998 Vol 23, No 4. Optics Letters. pp 247-249

3.3 “Intercavity Rayleight scattering in microspheres: limits imposed on quallity factor and mode coupling” M. L. Gorodetsky, V. S. Ilchenko, A. D. Pryamkiov, from Rep.3611-08 at the Laser Resonators Symposium, Photonics West’99, San-Jose CA, Jan.23-29, 1999. Submitted to JOSA B.

3.4 “Splitting of high Q Mie modes induced by light backscattering in silica microspheres”, D. S. Weiss, V. Sandoghdar, J. Hare, V. Lefevre-Seguin, J.M. Raimond, and S. Haroche, Optics letters Vol 20, No 18 Sept 15, 1995.

3.5 “Splitting of low Q Mie resonances”, Lawreence A. Ferrari and Joseph B. Comunale, JOSA A, Vol 15, No 7, July 1998.

3.6 “Instumentation for the stable operation of laser diodes”, C. C. Bardley, J. Chen, and Randall G. Hulet, Rev. Sci. Instrum 61 (8) August 1990. pp2097-2100.

3.7 “A low noise high speed diode laser current controller”, K. G. Libbrecht, J. L. Hall, Rev. Sci Instrum 64 (8) August 1993. p2133-2135

3.8 “Teaching physics with 670 nm diode lasers. Construction of stabilized lasers and Lithium cells”, KG Libbrecht, R A Boyd, P. A. Willems, T. L. Gustavson, D. K. KIM, American Journal of Physics 63: (8) pp. 729-737 August 1995.

3.9 “Very high-Q whispering gallery mode resonances observed in fused silica”, L. Collot, V lefervre-Seguin, M Brune, J M Raimond and S. Haroche Europhys letters 23 (5), pp 327-334 (1993)

3.10 “Classical Electrodynamics” by J. D. Jackson, 2nd Ed. Wiley 1975

Color Plate

Erik Streed, Senior Thesis

Figure 3.1.a. Clean silica.

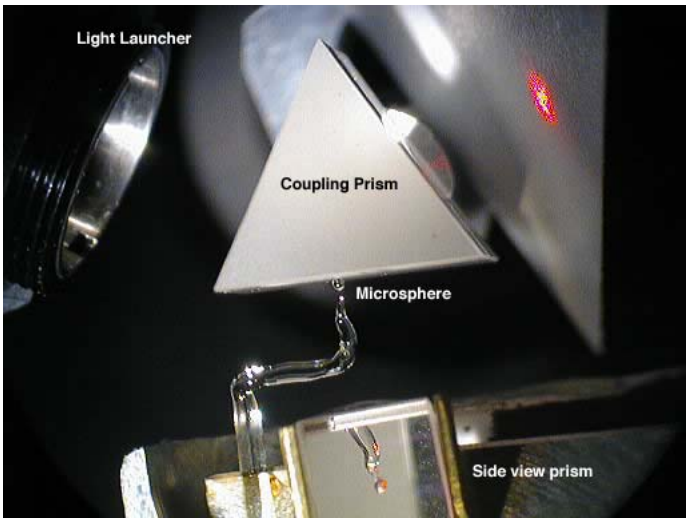

Fig 3.2 Experimental Coupling Setup

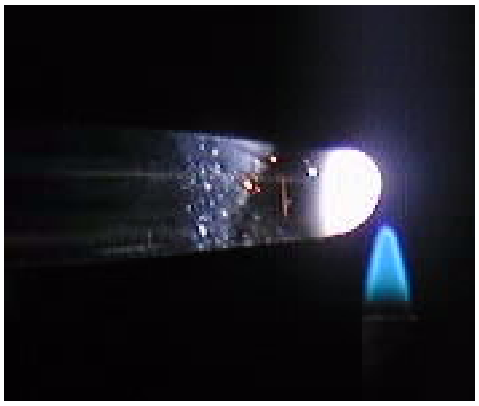

Figure 3.1.b. Dirtysilica.

Fig. 3.3.a. Microsphere WGM illuminated by dust.

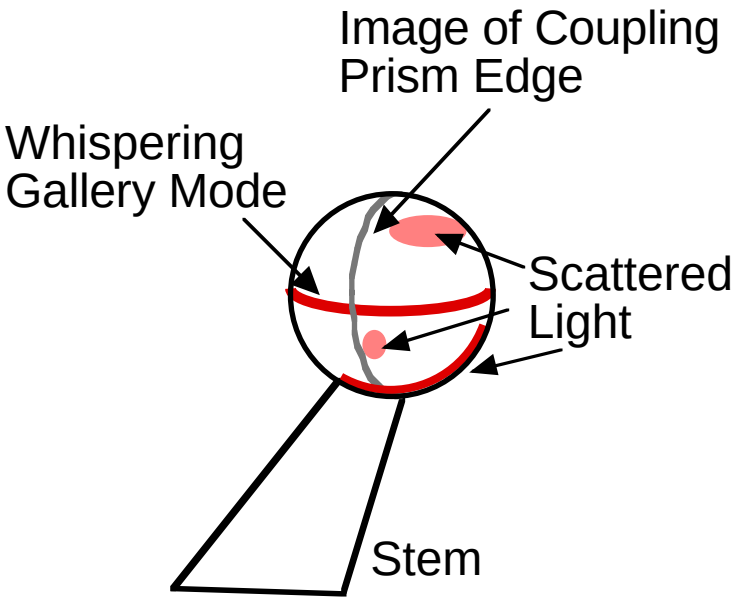

Fig 3.3.b. Diagram of Fig 3.3.a.